

Superfluidity of Dense ^4He in Vycor

Saad A. Khairallah¹ and D. M. Ceperley²

¹Dept. of Physics, University of Illinois at Urbana-Champaign, Urbana, IL 61801, USA

²NCSA and Dept. of Physics, University of Illinois at Urbana-Champaign, Urbana, IL 61801, USA

To understand the recent experiments of Kim and Chan which find a superfluid-like response in dense ^4He , we calculate properties of a model of ^4He in Vycor using the Path Integral Monte Carlo method. We find that ^4He forms a distinct layered structure. The first layer is solid-like and highly localized. The second layer is disordered: some atoms are not localized and they could give rise to the observed superfluid response. Higher layers are then nearly perfect crystals and only participate in the superfluidity in so far as they are close to the second layer. The addition of a single ^3He atom was enough to bring down the total superfluidity because it goes into the second layer and blocks the exchange in that layer. Our results are consistent with the persistent liquid layer model to explain the observations.

A supersolid[1, 2, 3, 4] is a proposed phase of a quantum system in which long-range crystalline order and superfluidity coexist. Attempts to observe supersolid behavior in solid ^4He were not successful [5] until recently: Kim and Chan reported the observation of a supersolid Helium phase, in porous Vycor [6] and more recently in bulk solid ^4He [7]. We focus here on the measurements of the Helium-Vycor system. Related calculations on bulk solid ^4He are discussed elsewhere [8].

The occurrence of supersolid behavior in Vycor, a disordered porous glass, can be understood from the properties of Vycor. Chan suggested that the complex Vycor geometry stabilizes mobile defects. At the low temperatures (experimentally at 175mK), defects could condense into a coherent state, and superflow would result. Kim and Chan pressurized their cell to 60 Bars, substantially above the believed freezing pressure for helium in Vycor estimated at 40 bars. However, even if most of the helium is solid, it is not clear if there remains a liquid film near the Vycor-helium surface even at these pressures. The film could arise from the mismatch of lattice parameters as the density of ^4He varies from the center of the pores to their surface.

In order to understand the Kim-Chan experiment, in particular to see what is happening at the microscopic level, we propose a model of the helium-Vycor system and calculate its properties with the Path Integral Monte Carlo(PIMC) method reviewed in [9]. Path Integral Monte Carlo can calculate exact thermodynamic properties of bosonic systems such as ^4He at non-zero temperature by sampling the thermal density matrix $\rho \equiv e^{-\beta H}$, with $\beta = 1/k_B T$ and H the Hamiltonian. An explicit expression for the density matrix is obtained by expanding into a path and approximating the higher temperature density matrices($\tau = M/\beta$). Bose statistics are obtained by symmetrizing the density matrix $\rho_{Bose}(R, R'; \beta) = \sum_P \rho(R, PR'; \beta)$. PIMC proved accurate in studying properties in the normal liquid, superfluid and crystal phase [10, 11, 12]. In contrast to methods based on trial wavefunctions, in PIMC only the Hamiltonian enters, so no biases are made on the struc-

ture of the many-body system.

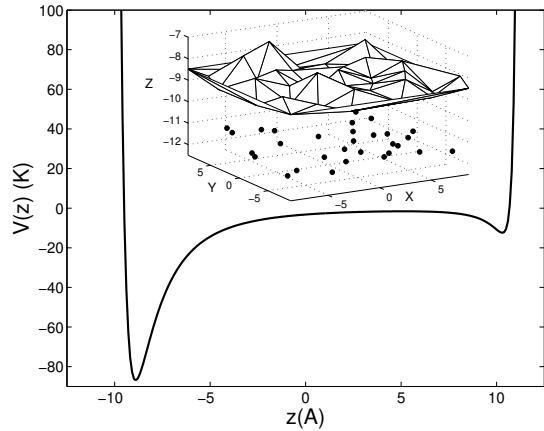


FIG. 1: The external potential $V(z)$ experienced by the helium atoms in “cell 2”. The Vycor is on the left side ($z= -12.5\text{\AA}$) and solid helium on the right side ($z=12.5\text{\AA}$). The inset is a 3D representation of the rough Vycor surface: the black dots are the positions of the Vycor impurities placed randomly at 1\text{\AA} away from the Vycor wall. The rugged surface shows the positions of the helium atoms (located at the vertices) in the first layer.

Vycor’s complex geometry is difficult to simulate directly. Under the transmission electron microscope, Vycor shows interconnected pores with diameters between 60\AA and 80\AA and a length of 300\AA , with a narrow distribution of pore sizes. Current simulation techniques treating all the atoms (roughly 30000 atoms/pore) with PIMC are unable to simulate even a single pore. It is thought that above the freezing pressure (40 bars) a ^4He crystal will occupy the center of a pore [13]. Previous PIMC calculations have found that a perfect crystal will not have a superfluid response at long wavelength [8]. Making this assumption, we study only the region near the surface of a pore and model it with the slab geometry: our simulation cell is periodic in both the x and y directions. In the negative z-direction there is a wall, representing bulk Vycor on top of which are placed Vy-

cor “particles” in random positions 1 Å above the flat Vycor surface. These particles serve to make the surface rough and break translational invariance. In the positive z -direction is a wall which models bulk solid Helium at a pressure of 62 bars(see Fig. 1) .

The main input to PIMC is the interaction potential between various particles. We assume that the Helium-Helium interaction is given by the Aziz [14] potential which has been used within PIMC to study numerous other properties of helium and gives energies accurate to about 1% of the bulk binding energy. The potential between helium and the upper wall was derived by integrating an approximate LJ 6-12 potential ($\epsilon = 10.22K$ and $\sigma = 2.556\text{\AA}$) over the volume $z > 11.7\text{\AA}$ (cell 1) resulting in a LJ (3-9) potential.

We also assume helium-Vycor surface interaction is a LJ (3-9) potential [15]: $V(z) = \frac{D}{2}[(\frac{z_e}{z})^9 - 3(\frac{z_e}{z})^3]$. Since Vycor glass, SiO_2 , should behave similarly to MgO [16], we pick the well depth to be $D = -86.9K$, and the range of the attraction, $z_e = 3.6\text{\AA}$. In order to pin the helium crystal in the xy plane and model the roughness of the Vycor, we add Vycor “particles” in random positions 1 Å above the wall. The interaction between the helium atoms and the Vycor particles is determined by demanding that a complete layer of the particles give the same LJ (3-9)potential; this is done by inverting the above equations. Experiments [17] show that the roughness in Vycor is on the scale of 0.8nm, not very different from what we have assumed. Figure 1 shows the wall potential and the surface roughness.

We set the helium density to match the experimental conditions by adjusting the number of helium atoms and the total area in the xy plane so that the helium density in the topmost layer matches that of solid ^4He at a target pressure close to 62 bars. We start the simulation with 221 atoms placed in 7 layers in an hexagonal closed packed solid phase. Each layer contains 30 atoms except for the first layer placed at the strongly attractive Vycor wall potential (Fig. 1). We have performed extensive simulations with two geometries, denoted as Cell 1 (221 He atoms with a box $17.75 \times 18.45 \times 23.4\text{\AA}^3$) and Cell 2 (221 atoms with a box $17.25 \times 17.93 \times 25\text{\AA}^3$). Cell 1 is roughly stress free, while Cell 2 provides us with a way to look at the model under anisotropic stress.

The density in the z -direction (see Fig. 2) shows a distinct layered structure of ^4He . The density increases as we approach the Vycor wall because of the stronger attraction of the potential well. The Vycor particles distort the shape of the density peak in the first layer because there are binding sites at different values of z . We find a perfect crystal is stable in the upper portion of the cell with a lattice constant of 3.55\AA in cell 1 and 3.45\AA in cell 2, at the target pressure of 62 bars. We estimate the pressure by calculating the density per layer from figure 2 and comparing it with the experimental equation

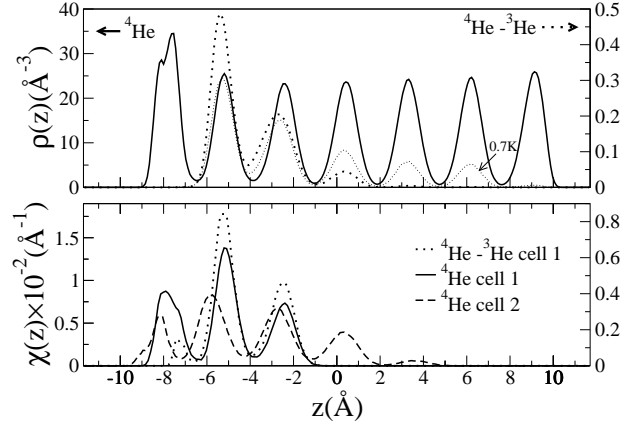


FIG. 2: The density and superfluid density as a function of z . The left scale (solid line) corresponds to pure ^4He and the right to the mixture: one ^4He atom replaced by a ^3He atom. Top: The density in the z -direction for cell 1 at 0.2K. The split peak in the first (leftmost) layer is due to the rough Vycor surface. The dotted lines show the ^3He density at 0.2K and 0.7K. Bottom: Local superfluid density of ^4He determined by recording which layers the winding paths visit. The local superfluid density of ^4He in the presence of the ^3He impurity is still prominent in the second layer.

of state[18].

We determine the spatial ordering within a layer with the structure factor in the x - y direction

$$S_n(\mathbf{k}) = \frac{1}{N} \langle \rho_n(\mathbf{k}) \rho_n(-\mathbf{k}) \rangle \quad (1)$$

where $\rho_n(\mathbf{k}) = \sum_{i=1}^N \Theta(z_i \in n) \exp(i\mathbf{k} \cdot \mathbf{r}_i)$ is the Fourier transform of the density within layer n and $\mathbf{k} = (k_x, k_y, 0)$. We can see the signature of a solid from the peak of $S(\mathbf{k})$ around $k_0 = 2.04\text{\AA}^{-1}$ as shown in figure 3 for cell 1; the peak clearly shows an hexagonal structure for layers three and above. The density profiles within a layer in Fig. 3 confirm this interpretation. However, not all of the layers are solid. In fact, layer one is solid-like with the helium atoms well-localized but with their mean positions highly constrained by the underlying disorder. Layer 2 is more disordered and the atoms are out of registry with the first layer. Because the second layer density is lower, the atoms are much less localized and, as we shall see, are able to become superfluid. Layers three and above are quantum solids, mostly free of defects.

The superfluid fraction is computed in PIMC from the mean squared winding number [19],

$$\frac{\rho_s}{\rho} = \frac{m \langle W^2 \rangle}{2\beta \hbar^2 N} \quad (2)$$

where $\beta = 1/k_B T$ and N is the number of Helium atoms. The winding number is calculated according to $\mathbf{W} = \sum_{i,k} (\mathbf{r}_{i,k} - \mathbf{r}_{i,k+1})$, where the sum is over particles i , and time slices k . The superfluid fraction increases

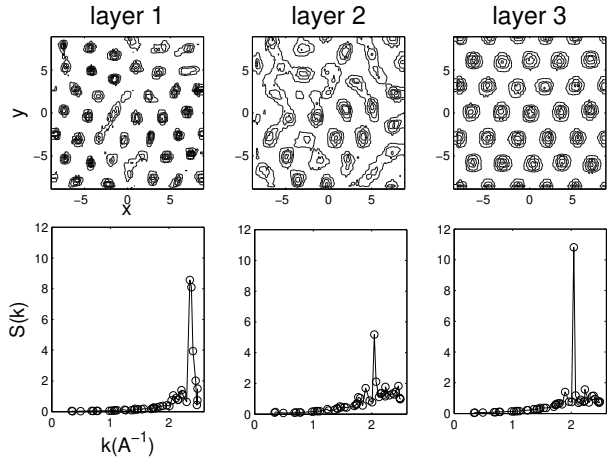


FIG. 3: Top: Contour plots of the helium density in the x-y plane in the first three layers at 0.2K for cell 1. In the first layer above the Vycor, the atoms are pinned by the strong Vycor interaction, in the second layer they are relatively delocalized, whereas the higher levels show a density distribution characteristic of bulk solid ^4He . Bottom: The layer-specific structure factor. The first layer has an amorphous structure, the second is still distorted but with a much smaller peak, while the third and higher layers have a single large peak at $k_o=2.04\text{\AA}^{-1}$ characteristic of a 2D quantum solid.

as we lower the temperature as shown in figure 4 and approaches values of about 4% below 0.3 K.

Before we confront experiment, we want to find the spatial distribution of the superfluid density. In principle, superfluidity is a global quantity; however, we can divide the winding number estimator into local contributions that sum to the total superfluid density [20]. The average superfluid density as a function of the distance above the Vycor wall $\chi(z)$ is:

$$\chi(z) = \frac{\sum_{k_{slice}, c_{cycle}} W_{k,c}^2 \delta(z_{k,c} - z)}{4\lambda\beta N} \quad (3)$$

satisfying,

$$\frac{\rho_s}{\rho} = \int dz \chi(z). \quad (4)$$

In figure 2, we show $\chi(z)$ for $T=0.2\text{K}$ in cell 1. One can see the layered structure of the density. Layer 2 has the largest superfluid component. Layer one contributes because of some ^4He atoms that are delocalized by Vycor impurities and sit close to layer 2. Layer 3 is also active. The superfluid response goes to zero above layer 3. However, this decay is quite slow in cell 2 where the two additional layers (4 and 5) still contribute to ρ_s/ρ .

To compare with experiment we must make two corrections; first that our model has a larger number of atoms closer to the Vycor surface area than experiment, and second that our cell has no tortuosity: the experimental path length for a superflow is greater than the

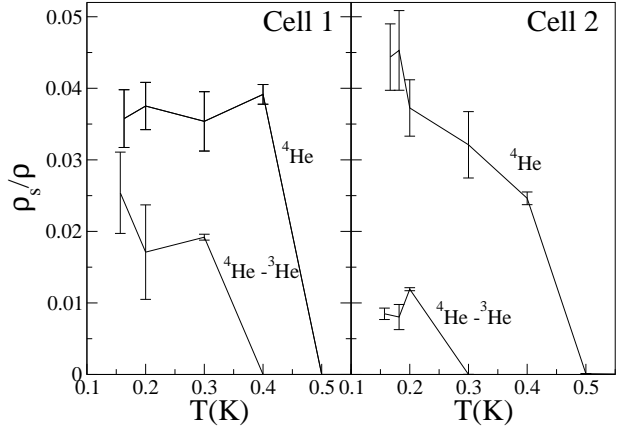


FIG. 4: The superfluid fraction ρ_s/ρ vs. temperature. The upper curve is for pure ^4He . The lower curve is for a mixture (one ^4He atom replaced by a ^3He atom).

straight line distance. We correct for the difference in Vycor surface area by assuming that the superfluidity is confined to a finite distance above the Vycor so that the effective number of atoms that do not respond to the moving boundaries is: $N_s = \sigma A$ where A is the Vycor surface area (actually the surface area of the mobile layer). We find that the maximum number of superfluid atoms per unit area is: $\sigma \approx 2.7\text{nm}^{-2}$. Then for a Vycor sample with experimental surface area per unit volume of $a = 0.2\text{nm}^{-1}$ the relative superfluid response would be $a\sigma_s/\mu\rho\kappa$ where $\mu = 0.3$ is the experimental Vycor sample pore fraction, $\kappa = 5$ is the tortuosity, and $\rho = 31.66\text{atom/nm}^{-3}$ is the solid number density. Using the characterization of Vycor, we would predict a measured superfluid fraction of 0.011. In fact, Kim and Chan measure a value two times smaller than this. One important effect missing in our calculation is that the supercurrents must tunnel through various weak links, an aspect not in our calculations because of the limited extent of the cell in the x-y directions. In addition, we have not taken the thermodynamic limit, though it is not obvious how to do this without a better model of the Vycor. In any case, Kim and Chan's measured values are well within the range expected from our calculations.

Kim and Chan also studied the effect of ^3He impurities on the measurement of the superfluid density. Accordingly, we replaced a single ^4He with a ^3He atom. (Note that we do not need to consider fermi statistics for a single fermion). This corresponds to roughly 0.3% concentration of ^3He (assuming our cell size is $\approx 2/3$ of the pore). Experimentally, this concentration was enough to destroy any “supersolid” response. The mass difference between ^3He and ^4He , giving a larger kinetic energy, causes the ^3He path to occupy more space than a ^4He atom. This extra space is available in the second layer. The ^3He atom is not allowed to exchange with the ^4He and thus will locally reduce the superfluid density. Since

the impurity did not always find the most favorable configuration, *i.e.* one with lowest energy, we devised a new move that swapped the identity of the impurity with a random ^4He particle at a given frequency. This procedure quickly reached equilibrium.

The density profiles show that the ^3He impurity preferentially goes to the same site where the superfluidity is maximized (Fig. 2). At higher temperatures, it tunnels to other layers with an excitation energy of 0.8K. As the temperature is lowered, two competing effects take place. The ^4He atoms closest to the Vycor wall exchange causing superfluidity. However, the ^3He atom migrates towards the most superfluid layers, hence diminishing the total response of the system. The dense first layer has an insignificant density of ^3He . In figure 4, it caused a general decrease in total superfluidity and a shift towards a lower transition temperature. It is plausible that in a larger cell, an even smaller concentration of ^3He could pinch off the winding exchanges (or supercurrent) by going to choke positions not present in our small cell, thus giving better agreement with the experimental findings of a critical ^3He concentration of 0.1%.

Our results show superfluidity localized in specific layers of ^4He above the Vycor surface. We obtain a superfluid response about 2 times what is observed, but the difference is likely due to the very small simulation cells we used which do not have the full range of the random disorder. It is found that ^3He impurities gravitate to the same spatial locations as the superfluid density, thus poisoning the effect. Based on these simulations, the “persistent liquid film” interpretation of the Kim-Chan experiment seems not to be ruled out.

Kim and Chan[6] mention two pieces of evidence to argue against the liquid film interpretation. First, the observed temperature dependance of the superfluid density is unlike that of films. However, the films under pressure are totally enclosed within a solid and they are not like films forming an interface between a solid and a vacuum; as we have seen, there are low energy excitations giving rise to pronounced temperature effects, not present in the later case. Also, the connectivity of these new films could be different; it is likely that they are gossamer, as opposed to the robust films resulting when the pores are only partially filled. The second effect mentioned by Kim and Chan is the poisoning by small amounts of ^3He .

This does not happen in free films because the ^3He atom could be located above the plane of the ^4He film and thus not be effective in preventing ^4He exchanges. Also, there are less likely to be choke points where a small amount of ^3He can kill an entire exchange path. Further studies with larger cells and more realistic disorder are needed to firm up these conclusions.

Thanks to J. Kim for computational advice and discussions with M. Chan and M. Cole. Computer time has been provided by NCSA (Illinois), MCC (Illinois) and PSC (Pennsylvania). This work was supported by NSF and the fundamental physics program at NASA (NAG-8-1760).

- [1] O. Penrose, L. Onsager, Phys. Rev. **104**, 576 (1956).
- [2] A. F. Andreev and I. M. Lifshitz, Sov. Phys. JETP **29**, 1107 (1969).
- [3] A. J. Leggett, Phys. Rev. Lett. **25**, 1543 (1970).
- [4] G. V. Chester, Phys. Rev. A **2**, 256 (1970).
- [5] Mark W. Meisel, Physica B **178**, 121 (1992).
- [6] E. Kim and M. H. Chan, Nature **427**, 225 (2004).
- [7] E. Kim and M. H. Chan, Science **305**, 1941 (2004).
- [8] D. M. Ceperley and B. Bernu, Phys. Rev. Letts. **93**, 155303 (2004).
- [9] D. M. Ceperley, Rev. Mod. Phys. **67**, 279 (1995).
- [10] E. L. Pollock and D. M. Ceperley, Phys. Rev. B **30**, 2555 (1984).
- [11] D. M. Ceperley and E. L. Pollock, Phys. Rev. Lett. **56**, 351 (1986).
- [12] E. W. Draeger and D. M. Ceperley, Phys. Rev. B **61**, 12094 (2000).
- [13] D. F. Brewer, J. Rajendra, N. Sharma, A. L. Thomson and Jin Xin, Physica B **165** & **166**, 551 (1990).
- [14] Ronald A. Aziz, Alec R. Janzen and Micheal R. Moldover, Phys. Rev. Lett. **74**, 1586 (1995).
- [15] M. W. Cole, T. T. Tsong, Surf. Sci. **69**, 325-35 (1977).
- [16] C. H. Anderson and E. S. Sabisky, Phys. Rev. Lett. **24**, 1049 (1970).
- [17] P. Levitz, G. Ehrest, S. K. Sinha and J. M. Drake, J. Chem. Phys. **95**, 6151 (1991).
- [18] A. Driessens, I. F. Silvera and E. van der Poll, Phys. Rev. B **33**, 3269 (1986).
- [19] E. L. Pollock and D. M. Ceperley, Phys. Rev. B **36**, 8343 (1987).
- [20] E. W. Draeger and D. M. Ceperley, Phys. Rev. Lett. **90**, 65301 (2003).